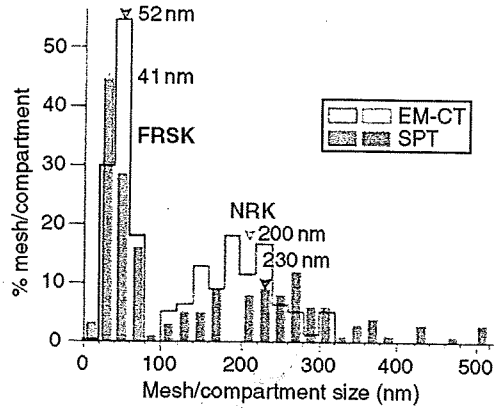


**Fig. 11** Comparison of the distributions of the MSK mesh size on the cytoplasmic surface of the plasma membrane estimated by electron tomography (open bars), with that of the compartment size determined from the phospholipid diffusion data (closed bars, adapted from Fujiwara *et al.* (2002) and Murase *et al.* (2004)), for NRK (magenta) and FRSK (blue) cells. Within the same cell type, the MSK mesh size and the diffusion compartment size exhibited similar distributions (compare the open and closed bars with the same color). The actual sizes are quite different between NRK and FRSK cells. Reproduced from Morone *et al.* (2006). © 2003 The Rockfeller University Press.

for each domain was measured by the AMIRA software. The distributions of the square root of the area size (the side length, assuming a square shape for the area) for NRK (magenta open bars) and FRSK (blue open bars) cells are shown in Fig. 11. The median values of the area and its square root are $3.9 \times 10^4$ nm$^2$ and 200 nm, respectively, for NRK cells, and $2.7 \times 10^3$ nm$^2$ and 52 nm, respectively, for FRSK cells.

### F. Comparison of the MSK Mesh Size on the Plasma Membrane Determined by Electron Tomography with the Compartment Size for Membrane Molecule Diffusion

Our group has proposed that a part of the MSK is directly and closely associated with the cytoplasmic surface of the plasma membrane, and that this close association of parts of the MSK meshwork induces partitioning of the plasma membrane, with regard to the translational diffusion of membrane molecules, based on high speed single-particle tracking data for membrane proteins and lipids (Fig. 12, Jacobson *et al.*, 1995; Kusumi and Sako, 1996; Kusumi *et al.*, 2005b). Namely, the entire plasma membrane is parceled up into apposed domains by the MSK meshwork associated with the plasma membrane. In the short-time regime, these

micrographs of the plasma membrane samples. The same view fields as those in A. (Row C) The areas delimited by the actin filaments closely apposed to the cytoplasmic surface of the cell membrane are shown. Different colors are used to aid in visualization. Reproduced from Morone *et al.* (2006). © 2003 The Rockfeller University Press. (See Color Plate no. 8 in the Color Plate Section.)

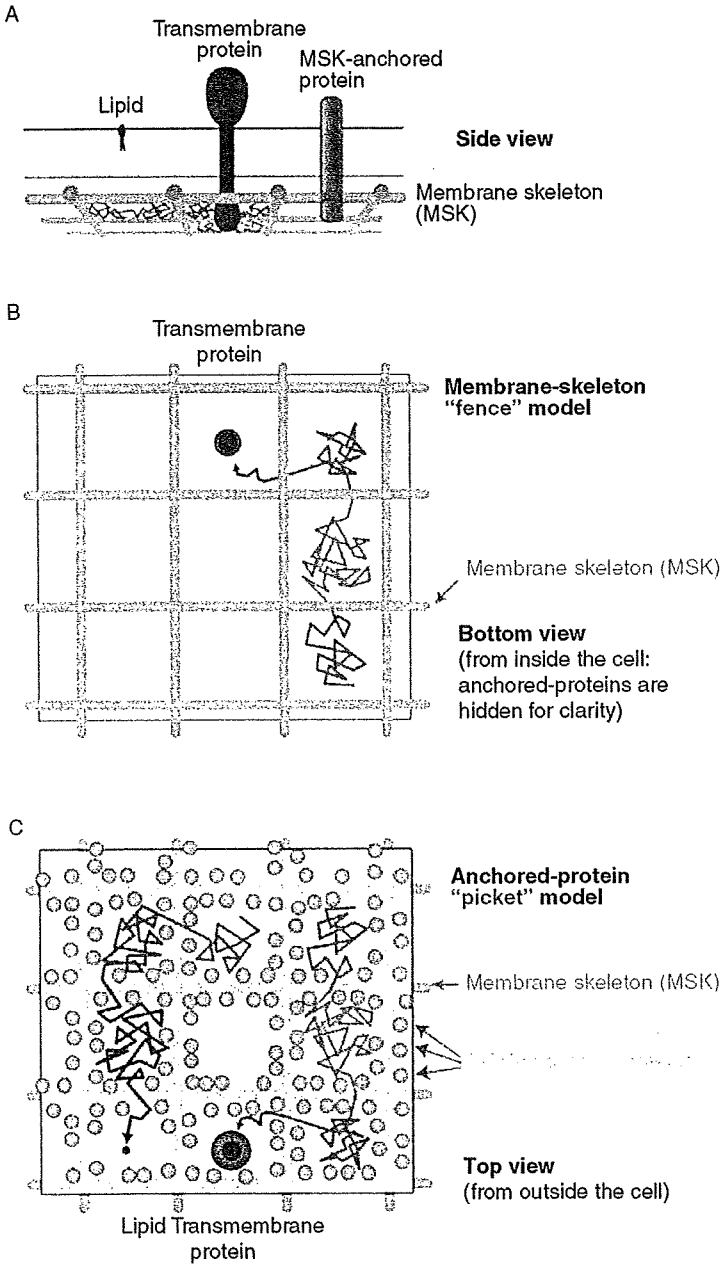


**Fig. 12** Proposed mechanisms for the compartmentalization of the plasma membrane for the translational diffusion of transmembrane proteins and phospholipids (located in the *outer* leaflet) in the membrane: Corralling by the membrane-skeleton "fences" and the anchored-protein "pickets". The plasma membrane may be parceled up into closely apposed domains (compartments) for the translational diffusion of transmembrane proteins and lipids (even those located in the outer leaflet).

membrane molecules are temporarily confined within the compartments delimited by the MSK mesh, and, in the long-time regime, they undergo macroscopic diffusion by hopping between these compartments. The Singer-Nicolson model of the membrane is only suitable for a description of diffusion on the scale of ~10 nm in the plasma membrane, but the presence of such compartment boundaries must be considered for the diffusion over distances of several 10 s of nanometers.

Transmembrane proteins are temporarily confined within a compartment, due to the collision of their cytoplasmic domains with the actin filaments in the MSK mesh, closely located on the surface of the plasma membrane (MSK-"fence" model, Fig. 12; also see Sako and Kusumi, 1995; Sako *et al.*,1998; Suzuki *et al.*, 2005; Tomishige *et al.*, 1998).

Lipid molecules also undergo hop diffusion, which might be explained by the "anchored-protein picket model" (Fujiwara *et al.*, 2002; Kusumi *et al.*, 2005b; Murase *et al.*, 2004). In this "picket" model, various transmembrane proteins anchored to and aligned along the actin filaments that are located right on the cytoplasmic surface of the plasma membrane might effectively act as rows of pickets against the free diffusion of all of the molecules incorporated in the cell membrane. This is due to the steric hindrance and circumferential slowing of the immobile picket proteins, anchored to and lined up along the MSK. Here, the circumferential slowing due to the hydrodynamic friction-like effect of the immobile picket proteins (Bussell *et al.*, 1995a,b) is critical for effectively blocking the passage of membrane molecules across the picket line, because this effect will propagate quite far from the immobile protein surface. Without this effect, the picket model would not be valid. Lipid movement is affected only by pickets, whereas both pickets and fences would act on transmembrane proteins.

The size distributions of the compartments for the diffusion of membrane molecules were obtained for an unsaturated phospholipid, L-α-dioleoylphosphatidylethanolamine, by Fujiwara *et al.* (2002) and Murase *et al.* (2004), for NRK and FRSK cells, respectively. The distributions of the side lengths for NRK (magenta closed bars) and FRSK (blue closed bars) cells are shown in the histograms in Fig. 12. The median values of the compartment area and the side length are $4.3 \times 10^4$ nm$^2$ and 230 nm, respectively, for NRK cells, and $2.1 \times 10^3$ nm$^2$ and 41 nm, respectively, for FRSK cells (Murase *et al.*, 2004).

---

All of the membrane constituent molecules undergo short-term confined diffusion within a compartment and long-term hop diffusion between these compartments. This may be due to corralling by two mechanisms: The membrane-skeleton "fences" and the anchored-protein "pickets". (A) Side-view schematic representation of a transmembrane protein, a phospholipid located in the outer leaflet, and an MSK-anchored protein (membrane skeleton-anchored protein, grey cylinder). The former two molecules are mobile, whereas the MSK-anchored protein is immobile. (B) The membrane-skeleton "fence" or "corral" model, showing that transmembrane proteins are confined within the mesh of the actin-based membrane skeleton, as viewed from inside the cell. Meanwhile the phospholipids located in the outer leaflet of the membrane do not directly interact with the membrane skeleton. (C) The anchored-protein "picket" model, showing the MSK-anchored proteins effectively represent immobile obstacles to the diffusion of transmembrane proteins and phospholipids, as viewed from outside the cell. (See Color Plate no. 9 in the Color Plate Section.)

These results indicate that in the same cell line (for both the NRK and FRSK cases), the MSK mesh size determined by electron tomography and the diffusion compartment size determined by the high-speed single-particle tracking of a phospholipid are similar to each other. However, between these two cell lines, both the MSK mesh and the diffusion compartment sizes differ greatly. The similarities between the MSK mesh sizes and the diffusion compartment sizes in cell lines that exhibit quite different distributions strongly support the MSK fence and picket models.

## IV. Electron Tomography Clarified that Some of the Actin Filaments are Laterally Bound to the Cytoplasmic Surface of the Plasma Membrane

Many mammalian cells have a well-developed cytoskeleton in the bulk cytoplasm. The cytoskeleton consists of actin filaments, intermediate filaments, such as keratin filaments and neurofilaments, and microtubules. Since actin filaments are more involved in cell movement and morphological changes of the cell than the others, they have been believed to be associated with the plasma membrane, at least in the regions of leading edges and membrane ruffles. However, since the interactions of the actin filaments with the plasma membrane have traditionally been investigated in this context, in the actin literature, researchers have almost always assumed that, to understand their interactions, it is sufficient to consider that the barbed-ends of the actin filaments are bound to the plasma membrane, and that they can neglect the lateral binding of the actin filaments to the components of the plasma membrane.

In the late 1980s, actin binding and nucleation on the cytoplasmic surface of the plasma membrane were investigated (Schwartz and Luna, 1986, 1988; Tranter *et al.*, 1989), and ponticulin, a transmembrane protein in the Dictyostelium discoideum plasma membrane that laterally binds to actin filaments, was discovered (Wuestehube and Luna, 1987). Since then, biochemical analyses have revealed many more proteins that exhibit lateral binding to the actin filaments as well as binding to membranes and membrane molecules. These proteins include the Ezrin/Radixin/Moesin (ERM)-family of proteins (Hamada *et al.*, 2003; James *et al.*, 2001), the villin-gelsolin-superfamily proteins including fimbrin and supervillin (Pestonjamasp *et al.*, 1997, where the involvement of supervillin in adhesion structures is described), Epithelial protein lost in neoplasm (EPLIN), which binds to the cadherin-catenin complex (Abe and Takeichi, 2008; Maul *et al.*, 2003), filamin, which is involved in various membrane-protein functions (Stossel *et al.*, 2001; Tavano *et al.*, 2006; Uribe and Jay, 2007), dystrophin and utrophin, which, like tropomyosin, are likely to bind to actin filaments (Fig. 1; Rybakova and Ervasti, 1997; Rybakova *et al.*, 2002), and, let us not forget the myosin-family of proteins, including myosin-I. Namely, *these proteins are likely to mediate the lateral binding of*

*actin filaments to the cytoplasmic surface of the plasma membrane*, and thus *lateral binding as well as barbed-end binding* is important for understanding the MSK functions and the interaction between the plasma membrane and the cytoskeleton.

However, very few systematic structural studies of the MSK at the interface with the plasma membrane have been carried out. The actin filaments laterally bound to the plasma membrane have not received sufficient attention, despite their possibly important functions. This is partly due to the technical difficulties in obtaining large plasma membrane specimens that allow high resolution observations, without introducing too many artifacts. We think that 3D reconstructions of the MSK, using electron tomography with frozen-etched, platinum-replicated plasma membrane specimens, may be ideal for carrying out ultrastructural observations of the interface between the MSK and the plasma membrane. We hope that this review enhances the readers' interests in the interface structures between the MSK and the plasma membrane, and that the methods described in this review will help the readers to perform electron microscopic as well as tomographic studies of the interactions of the MSK with the plasma membrane.

## Acknowledgments

We would like to thank Shigeki Yuasa and John Heuser for their helpful advice and encouragement throughout this electron tomography work. This work was supported in part by World Premier International Research Center Initiative (WPI initiative) of the Ministry of Education, Culture, Sports, Science, and Technology (MEXT) of the Japanese government, and also by Health Labor Sciences Research Grant nano-001 to N. Morone, and Grants-in-Aid for Scientific Research and that on Priority Areas from the MEXT to J. Usukura and A. Kusumi.

## References

Abe, K., and Takeichi, M. (2008). EPLIN mediates linkage of the cadherin catenin complex to F-actin and stabilizes the circumferential actin belt. *Proc. Natl. Acad. Sci. USA* **105,** 13–19.

Bennett, V. (1990). Spectrin-based membrane skeleton: A multipotential adaptor between plasma membrane and cytoplasm. *Physiol. Rev.* **70,** 1029–1065.

Bussell, S. J., Koch, D. L., and Hammer, D. A. (1995a). Effect of hydrodynamic interactions on the diffusion of integral membrane proteins: Tracer diffusion in organelle and reconstituted membranes. *Biophys. J.* **68,** 1828–1835.

Bussell, S. J., Koch, D. L., and Hammer, D. A. (1995b). Effect of hydrodynamic interactions on the diffusion of integral membrane proteins: Diffusion in plasma membranes. *Biophys. J.* **68,** 1836–1849.

Byers, H. R., and Porter, K. R. (1977). Transformations in the structure of the cytoplasmic ground substance in erythrophores during pigment aggregation and dispersion. I. A study using whole-cell preparations in stereo high voltage electron microscopy. *J. Cell Biol.* **75,** 541–558.

Byers, T. J., and Branton, D. (1985). Visualization of the protein associations in the erythrocyte membrane skeleton. *Proc. Natl. Acad. Sci. USA* **82,** 6153–6157.

Chandler, D. E., and Heuser, J. (1979). Membrane fusion during secretion: Cortical granule exocytosis in sex urchin eggs as studied by quick-freezing and freeze-fracture. *J. Cell Biol.* **83,** 91–108.

Choquet, D., Felsenfeld, D. P., and Sheetz, M. P. (1997). Extracellular matrix rigidity causes strengthening of integrin-cytoskeleton linkages. *Cell* **88,** 39–48.

Coleman, T. R., Fishkind, D. J., Mooseker, M. S., and Morrow, J. S. (1989). Functional diversity among spectrin isoforms. *Cell Motil. Cytoskeleton* **12,** 225–247.

Edidin, M., Kuo, S. C., and Sheetz, M. P. (1991). Lateral movements of membrane glycoproteins restricted by dynamic cytoplasmic barriers. *Science* **254,** 1379–1382.

Evans, E. A. (1989). Structure and deformation properties of red blood cells: Concepts and quantitative methods. *Meth. Enzymol.* **173,** 3–35.

Fujimoto, K. (1995). Freeze-fracture replica electron microscopy combined with SDS digestion for cytochemical labeling of integral membrane proteins. Application to the immunogold labeling of intercellular junctional complexes. *J. Cell Sci.* **108**(Pt 11), 3443–3449.

Fujimoto, K., Umeda, M., and Fujimoto, T. (1996). Transmembrane phospholipid distribution revealed by freeze-fracture replica labeling. *J. Cell Sci.* **109**(Pt 10), 2453–2460.

Fujimoto, L. M., Roth, R., Heuser, J. E., and Schmid, S. L. (2000). Actin assembly plays a variable, but not obligatory role in receptor-mediated endocytosis in mammalian cells. *Traffic* **1,** 161–171.

Fujita, A., Cheng, J., Hirakawa, M., Furukawa, K., Kusunoki, S., and Fujimoto, T. (2007). Gangliosides GM1 and GM3 in the living cell membrane form clusters susceptible to cholesterol depletion and chilling. *Mol. Biol. Cell* **18,** 2112–2122.

Fujiwara, T., Ritchie, K., Murakoshi, H., Jacobson, K., and Kusumi, A. (2002). Phospholipids undergo hop diffusion in compartmentalized cell membrane. *J. Cell Biol.* **157,** 1071–1081.

Hainfeld, J. F., and Steck, T. L. (1977). The sub-membrane reticulum of the human erythrocyte: A scanning electron microscope study. *J. Supramol. Struct.* **6,** 301–311.

Hamada, K., Shimizu, T., Yonemura, S., Tsukita, S., and Hakoshima, T. (2003). Structural basis of adhesion-molecule recognition by ERM proteins revealed by the crystal structure of the radixin-ICAM-2 complex. *EMBO J.* **22,** 502–514.

Hanson, P. I., Roth, R., Lin, Y., and Heuser, J. E. (2008). Plasma membrane deformation by circular arrays of ESCRT-III protein filaments. *J. Cell Biol.* **180,** 389–402.

Hanson, P. I., Roth, R., Morisaki, H., Jahn, R., and Heuser, J. E. (1997). Structure and conformational changes in NSF and its membrane receptor complexes visualized by quick-freeze/deep-etch electron microscopy. *Cell* **90,** 523–535.

Hartwig, J. H., Chambers, K. A., and Stossel, T. P. (1989). Association of gelsolin with actin filaments and cell membranes of macrophages and platelets. *J. Cell Biol.* **108,** 467–479.

Heuser, J. (2005). Deep-etch EM reveals that the early poxvirus envelope is a single membrane bilayer stabilized by a geodetic "honeycomb" surface coat. *J. Cell Biol.* **169,** 269–283.

Heuser, J. E. (1983). Procedure for freeze-drying molecules adsorbed to mica flakes. *J. Mol. Biol.* **169,** 155–195.

Heuser, J. E. (2000). Membrane traffic in anaglyph stereo. *Traffic* **1,** 35–37.

Heuser, J. E., and Anderson, R. G. (1989). Hypertonic media inhibit receptor-mediated endocytosis by blocking clathrin-coated pit formation. *J. Cell Biol.* **108,** 389–400.

Heuser, J. E., and Kirschner, M. W. (1980). Filament organization revealed in platinum replicas of freeze-dried cytoskeletons. *J. Cell Biol.* **86,** 212–234.

Heuser, J. E., Reese, T. S., Dennis, M. J., Jan, Y., Jan, L., and Evans, L. (1979). Synaptic vesicle exocytosis captured by quick freezing and correlated with quantal transmitter release. *J. Cell Biol.* **81,** 275–300.

Hirokawa, N., and Heuser, J. E. (1981). Quick-freeze, deep-etch visualization of the cytoskeleton beneath surface differentiations of intestinal epithelial cells. *J. Cell Biol.* **91,** 399–409.

Hirokawa, N., Tilney, L. G., Fujiwara, K., and Heuser, J. E. (1982). Organization of actin, myosin, and intermediate filaments in the brush border of intestinal epithelial cells. *J. Cell Biol.* **94,** 425–443.

Italiano, J. E., Jr., Lecine, P., Shivdasani, R. A., and Hartwig, J. H. (1999). Blood platelets are assembled principally at the ends of proplatelet processes produced by differentiated megakaryocytes. *J. Cell Biol.* **147,** 1299–1312.

Jacobson, K., Sheets, E. D., and Simson, R. (1995). Revisiting the fluid mosaic model of membranes. *Science* **268,** 1441–1442.

James, M. F., Manchanda, N., Gonzalez-Agosti, C., Hartwig, J. H., and Ramesh, V. (2001). The neurofibromatosis 2 protein product merlin selectively binds F-actin but not G-actin, and stabilizes the filaments through a lateral association. *Biochem. J.* **356,** 377–386.

Kajimura, N., Harada, Y., and Usukura, J. (2000). High-resolution freeze-etching replica images of the disk and the plasma membrane surfaces in purified bovine rod outer segments. *J. Electron Microsc. (Tokyo)* **49,** 691–697.

Kanaseki, T., Ikeuchi, Y., and Tashiro, Y. (1998). Rough surfaced smooth endoplasmic reticulum in rat and mouse cerebellar Purkinje cells visualized by quick-freezing techniques. *Cell Struct. Funct.* **23,** 373–387.

Kanaseki, T., Kawasaki, K., Murata, M., Ikeuchi, Y., and Ohnishi, S. (1997). Structural features of membrane fusion between influenza virus and liposome as revealed by quick-freezing electron microscopy. *J. Cell Biol.* **137,** 1041–1056.

Katayama, E. (1998). Quick-freeze deep-etch electron microscopy of the actin-heavy meromyosin complex during the *in vitro* motility assay. *J. Mol. Biol.* **278,** 349–367.

Katayama, E., Shiraishi, T., Oosawa, K., Baba, N., and Aizawa, S. (1996). Geometry of the flagellar motor in the cytoplasmic membrane of *Salmonella typhimurium* as determined by stereo-photogrammetry of quick-freeze deep-etch replica images. *J. Mol. Biol.* **255,** 458–475.

Kremer, J. R., Mastronarde, D. N., and McIntosh, J. R. (1996). Computer visualization of three-dimensional image data using IMOD. *J. Struct. Biol.* **116,** 71–76.

Kusumi, A., Ike, H., Nakada, C., Murase, K., and Fujiwara, T. (2005a). Single-molecule tracking of membrane molecules: Plasma membrane compartmentalization and dynamic assembly of raft-philic signaling molecules. *Semin. Immunol.* **17,** 3–21.

Kusumi, A., Nakada, C., Ritchie, K., Murase, K., Suzuki, K., Murakoshi, H., Kasai, R. S., Kondo, J., and Fujiwara, T. (2005b). Paradigm shift of the plasma membrane concept from the two-dimensional continuum fluid to the partitioned fluid: High-speed single-molecule tracking of membrane molecules. *Annu. Rev. Biophys. Biomol. Struct.* **34,** 351–378.

Kusumi, A., and Sako, Y. (1996). Cell surface organization by the membrane skeleton. *Curr. Opin. Cell Biol.* **8,** 566–574.

Landis, D. M., and Reese, T. S. (1981). Astrocyte membrane structure: Changes after circulatory arrest. *J. Cell Biol.* **88,** 660–663.

Lucic, V., Forster, F., and Baumeister, W. (2005). Structural studies by electron tomography: From cells to molecules. *Annu. Rev. Biochem.* **74,** 833–865.

Maul, R. S., Song, Y., Amann, K. J., Gerbin, S. C., Pollard, T. D., and Chang, D. D. (2003). EPLIN regulates actin dynamics by cross-linking and stabilizing filaments. *J. Cell Biol.* **160,** 399–407.

Medalia, O., Weber, I., Frangakis, A. S., Nicastro, D., Gerisch, G., and Baumeister, W. (2002). Macromolecular architecture in eukaryotic cells visualized by cryoelectron tomography. *Science* **298,** 1209–1213.

Merrifield, C. J., Feldman, M. E., Wan, L., and Almers, W. (2002). Imaging actin and dynamin recruitment during invagination of single clathrin-coated pits. *Nat. Cell Biol.* **4,** 691–698.

Mohandas, N., and Chasis, J. A. (1993). Red blood cell deformability, membrane material properties and shape: Regulation by transmembrane, skeletal and cytosolic proteins and lipids. *Semin. Hematol.* **30,** 171–192.

Moritz, M., Braunfeld, M. B., Guenebaut, V., Heuser, J., and Agard, D. A. (2000). Structure of the gamma-tubulin ring complex: A template for microtubule nucleation. *Nat. Cell Biol.* **2,** 365–370.

Morone, N., Fujiwara, T., Murase, K., Kasai, R. S., Ike, H., Yuasa, S., Usukura, J., and Kusumi, A. (2006). Three-dimensional reconstruction of the membrane skeleton at the plasma membrane interface by electron tomography. *J. Cell Biol.* **174,** 851–862.

Murase, K., Fujiwara, T., Umemura, Y., Suzuki, K., Iino, R., Yamashita, H., Saito, M., Murakoshi, H., Ritchie, K., and Kusumi, A. (2004). Ultrafine membrane compartments for molecular diffusion as revealed by single molecule techniques. *Biophys. J.* **86,** 4075–4093.

Nakata, T., and Hirokawa, N. (1992). Organization of cortical cytoskeleton of cultured chromaffin cells and involvement in secretion as revealed by quick-freeze, deep-etching, and double-label immunoelectron microscopy. *J. Neurosci.* **12,** 2186–2197.

Nermut, M. V. (1981). Visualization of the "membrane skeleton" in human erythrocytes by freeze-etching. *Eur. J. Cell Biol.* **25,** 265–271.

Ohno, S., and Takasu, N. (1989). Three-dimensional studies of cytoskeletal organizations in cultured thyroid cells by quick-freezing and deep-etching method. *J. Electron Microsc. (Tokyo)* **38,** 352–362.

Parton, R. G. (2003). Caveolae—from ultrastructure to molecular mechanisms. *Nat. Rev. Mol. Cell Biol.* **4,** 162–167.

Pestonjamasp, K. N., Pope, R. K., Wulfkuhle, J. D., and Luna, E. J. (1997). Supervillin (p205): A novel membrane-associated, F-actin-binding protein in the villin/gelsolin superfamily. *J. Cell Biol.* **139,** 1255–1269.

Qualmann, B., Kessels, M. M., and Kelly, R. B. (2000). Molecular links between endocytosis and the actin cytoskeleton. *J. Cell Biol.* **150,** F111–F116.

Rothberg, K. G., Heuser, J. E., Donzell, W. C., Ying, Y. S., Glenney, J. R., and Anderson, R. G. (1992). Caveolin, a protein component of caveolae membrane coats. *Cell* **68,** 673–682.

Rutter, G., Bohn, W., Hohenberg, H., and Mannweiler, K. (1988). Demonstration of antigens at both sides of plasma membranes in one coincident electron microscopic image: A double-immunogold replica study of virus-infected cells. *J. Histochem. Cytochem.* **36,** 1015–1021.

Rybakova, I. N., and Ervasti, J. M. (1997). Dystrophin-glycoprotein complex is monomeric and stabilizes actin filaments *in vitro* through a lateral association. *J. Biol. Chem.* **272,** 28771–28778.

Rybakova, I. N., Patel, J. R., Davies, K. E., Yurchenco, P. D., and Ervasti, J. M. (2002). Utrophin binds laterally along actin filaments and can couple costameric actin with sarcolemma when overexpressed in dystrophin-deficient muscle. *Mol. Biol. Cell* **13,** 1512–1521.

Sako, Y., and Kusumi, A. (1995). Barriers for lateral diffusion of transferrin receptor in the plasma membrane as characterized by receptor dragging by laser tweezers: Fence versus tether. *J. Cell Biol.* **129,** 1559–1574.

Sako, Y., Nagafuchi, A., Tsukita, S., Takeichi, M., and Kusumi, A. (1998). Cytoplasmic regulation of the movement of E-cadherin on the free cell surface as studied by optical tweezers and single particle tracking: Corralling and tethering by the membrane skeleton. *J. Cell Biol.* **140,** 1227–1240.

Sanan, D. A., and Anderson, R. G. (1991). Simultaneous visualization of LDL receptor distribution and clathrin lattices on membranes torn from the upper surface of cultured cells. *J. Histochem. Cytochem.* **39,** 1017–1024.

Sawada, Y., Tamada, M., Dubin-Thaler, B. J., Cherniavskaya, O., Sakai, R., Tanaka, S., and Sheetz, M. P. (2006). Force sensing by mechanical extension of the Src family kinase substrate p130Cas. *Cell* **127,** 1015–1026.

Schoenenberger, C. A., Steinmetz, M. O., Stoffler, D., Mandinova, A., and Aebi, U. (1999). Structure, assembly, and dynamics of actin filaments *in situ* and *in vitro*. *Microsc. Res. Tech.* **47,** 38–50.

Schwartz, M. A., and Luna, E. J. (1986). Binding and assembly of actin filaments by plasma membranes from Dictyostelium discoideum. *J. Cell Biol.* **102,** 2067–2075.

Schwartz, M. A., and Luna, E. J. (1988). How actin binds and assembles onto plasma membranes from Dictyostelium discoideum. *J. Cell Biol.* **107,** 201–209.

Sheetz, M. P. (2001). Cell control by membrane-cytoskeleton adhesion. *Nat. Rev. Mol. Cell Biol.* **2,** 392–396.

Sheetz, M. P., and Dai, J. (1996). Modulation of membrane dynamics and cell motility by membrane tension. *Trends Cell Biol.* **6,** 85–89.

Sheetz, M. P., Sable, J. E., and Dobereiner, H. G. (2006). Continuous membrane-cytoskeleton adhesion requires continuous accommodation to lipid and cytoskeleton dynamics. *Annu. Rev. Biophys. Biomol. Struct.* **35,** 417–434.

Stossel, T. P., Condeelis, J., Cooley, L., Hartwig, J. H., Noegel, A., Schleicher, M., and Shapiro, S. S. (2001). Filamins as integrators of cell mechanics and signalling. *Nat. Rev. Mol. Cell Biol.* **2,** 138–145.

Suzuki, K. G., Fujiwara, T. K., Edidin, M., and Kusumi, A. (2007a). Dynamic recruitment of phospholipase C gamma at transiently immobilized GPI-anchored receptor clusters induces IP3-$Ca^{2+}$ signaling: Single-molecule tracking study 2. *J. Cell. Biol.* **177,** 731–742.

Suzuki, K. G., Fujiwara, T. K., Sanematsu, F., Iino, R., Edidin, M., and Kusumi, A. (2007b). GPI-anchored receptor clusters transiently recruit Lyn and G alpha for temporary cluster immobilization and Lyn activation: Single-molecule tracking study 1. *J. Cell Biol.* **177,** 717–730.

Svitkina, T. M., Bulanova, E. A., Chaga, O. Y., Vignjevic, D. M., Kojima, S., Vasiliev, J. M., and Borisy, G. G. (2003). Mechanism of filopodia initiation by reorganization of a dendritic network. *J. Cell Biol.* **160,** 409–421.

Svitkina, T. M., Verkhovsky, A. B., and Borisy, G. G. (1995). Improved procedures for electron microscopic visualization of the cytoskeleton of cultured cells. *J. Struct. Biol.* **115,** 290–303.

Takeuchi, M., Miyamoto, H., Sako, Y., Komizu, H., and Kusumi, A. (1998). Structure of the erythrocyte membrane skeleton as observed by atomic force microscopy. *Biophys. J.* **74,** 2171–2183.

Tavano, R., Contento, R. L., Baranda, S. J., Soligo, M., Tuosto, L., Manes, S., and Viola, A. (2006). CD28 interaction with filamin-A controls lipid raft accumulation at the T-cell immunological synapse. *Nat. Cell Biol.* **8,** 1270–1276.

Tomishige, M., Sako, Y., and Kusumi, A. (1998). Regulation mechanism of the lateral diffusion of band 3 in erythrocyte membranes by the membrane skeleton. *J. Cell Biol.* **142,** 989–1000.

Tranter, M. P., Sugrue, S. P., and Schwartz, M. A. (1989). Evidence for a direct, nucleotide-sensitive interaction between actin and liver cell membranes. *J. Cell Biol.* **109,** 2833–2840.

Tsukita, S., and Ishikawa, H. (1980). Cytoskeletal network underlying the human erythrocyte membrane. Thin-section electron microscopy. *J. Cell Biol.* **85,** 567–576.

Uribe, R., and Jay, D. (2007). A review of actin binding proteins: New perspectives. *Mol. Biol. Rep.*

Ursitti, J. A., Pumplin, D. W., Wade, J. B., and Bloch, R. J. (1991). Ultrastructure of the human erythrocyte cytoskeleton and its attachment to the membrane. *Cell Motil. Cytoskeleton* **19,** 227–243.

Vertessy, B. G., and Steck, T. L. (1989). Elasticity of the human red cell membrane skeleton. Effects of temperature and denaturants. *Biophys. J.* **55,** 255–262.

Wuestehube, L. J., and Luna, E. J. (1987). F-actin binds to the cytoplasmic surface of ponticulin, a 17-kD integral glycoprotein from Dictyostelium discoideum plasma membranes. *J. Cell Biol.* **105,** 1741–1751.

Yin, H. L., and Hartwig, J. H. (1988). The structure of the macrophage actin skeleton. *J. Cell Sci. Suppl.* **9,** 169–184.

## Author Query

**Methods in Cell Biology, 88**
**Article No.: Chapter 12**

ELSEVIER

Dear Author,

During the preparation of your manuscript for typesetting some questions have arisen. These are listed below. Please check your typeset proof carefully and mark any corrections in the margin of the proof or compile them as a separate list. This form should then be returned with your marked proof/list of corrections to Elsevier Science.

**Disk use**

In some instances we may be unable to process the electronic file of your article and/or artwork. In that case we have, for efficiency reasons, proceeded by using the hard copy of your manuscript. If this is the case the reasons are indicated below:

☐ Disk damaged ☐ Incompatible file format ☐ LaTeX file for non-LaTeX journal

☐ Virus infected ☐ Discrepancies between electronic file and (peer-reviewed, therefore definitive) hard copy.

☐ Other: .....

We have proceeded as follows:

☐ Manuscript scanned ☐ Manuscript keyed in ☐ Artwork scanned

☐ Files only partly used (parts processed differently:.....)

**Bibliography**

If discrepancies were noted between the literature list and the text references, the following may apply:

☐ The references listed below were noted in the text but appear to be missing from your literature list. Please complete the list or remove the references from the text.

☐ Uncited references: This section comprises references which occur in the reference list but not in the body of the text. Please position each reference in the text or, alternatively, delete it. Any reference not dealt with will be retained in this section.

| Query Refs. | Details Required | Author's response |
|---|---|---|
| AU1 | Please provide the volume number and page range for the reference "Uribe and Jay, 2007" in the list. | |
| AU2 | Heuser and Salpeter, 1979 is not provided in the reference list. Please supply. | |
| AU3 | Suzuki *et al.*, 2005 is not provided in the reference list. Please supply. | |
| AU4 | Please check the chapter title. | |

Molecular and Cellular Neuroscience 39 (2008) 465–477

Contents lists available at ScienceDirect

Molecular and Cellular Neuroscience

journal homepage: www.elsevier.com/locate/ymcne

# Balanced expression of various TrkB receptor isoforms from the *Ntrk2* gene locus in the mouse nervous system

Haruko Kumanogoh *, Junko Asami, Shun Nakamura, Takayoshi Inoue

*Department of Biochemistry and Cellular Biology, National Institute of Neuroscience, National Center of Neurology and Psychiatry, 4-1-1 Ogawahigashi, Kodaira, Tokyo 187-8502, Japan*

ARTICLE INFO

*Article history:*
Received 21 March 2008
Revised 23 July 2008
Accepted 30 July 2008
Available online 9 August 2008

*Keywords:*
TrkB
BDNF
Alternative splicing
Antisense transcript
Mouse nervous system

ABSTRACT

A brain-derived neurotrophic factor (BDNF) receptor TrkB involves three spliced variants, namely the tyrosine kinase domain (TK) intact (+) and two TK(−) isoforms T1 and T2, yet their precise roles are largely unknown. Here we extensively map the mRNA expression patterns of BDNF and TrkB variants, further to gain insights in TK(−) specific functions during mouse development. Consequently, we found that TK(+), T1 and T2 were expressed in distinct regions of the mouse nervous system at the embryonic and postnatal stages, implicating separable functions of TK(−) forms. Additionally we uncovered five expressed segments in the intron between T2 and T1 specific exons, and one of these segments was revealed to code novel TK(−) receptors with unique responsiveness *in vitro*. These results suggest dynamic modes of expression from the *Ntrk2* gene locus and multiple roles of TK(−) forms in the developing mouse nervous system.



## Introduction

Brain-derived neurotrophic factor (BDNF) is a member of nerve growth factor (NGF) family that supports survival and differentiation of selected neuronal populations both in the central and peripheral nervous systems during development. BDNF is also known to play multiple roles in axonal pathfindings, dendritic growth and/or synaptic plasticity at the perinatal to adult stages (Bibel and Barde, 2000; Blum and Konnerth, 2005; Poo, 2001). In mice, for instance, three groups have independently generated *BDNF* gene knockout mice to reveal *in vivo* roles of BDNF (Conover et al., 1995; Ernfors et al., 1995; Jones et al., 1994; Liu et al., 1995) and found that *Bdnf*(−/−) mice are born alive but mostly died within 20 days after birth. They also realized abnormal behaviors of *Bdnf*(−/−) mice including difficulty in righting and spinning (Conover et al., 1995; Ernfors et al., 1995; Jones et al., 1994). At the tissue and cellular level, *Bdnf*(−/−) mice had massive cell loss in the peripheral sensory ganglia such as the dorsal root ganglia and trigeminal ganglia, while no significant cell loss was evident in the facial or spinal motor neurons. In contrast to the defects observed in the peripheral structures, no significant cytoarchitectural abnormalities were recognizable in the brain of knockout mice, although the mutant brain was smaller than control one (Conover et al., 1995). It was further found out that certain subpopulations of neurons were affected fully in differentiation (Itami et al., 2007; Jones et al., 1994), which suggests that BDNF is important in regulating differentiation of these neurons rather than cell survival. In human, accumulated evidence has indicated that *BDNF* mutations could be a causative factor of neurodegenerative disorders such as Alzheimer's, Huntington's and Parkinson diseases (Conover et al., 1995; Murer et al., 2001; Siegel and Chauhan, 2000; Zuccato and Cattaneo, 2007). Most recently, roles of alternative promoters in regulated expression BDNF have been elucidated, implicating context dependent activation of BDNF signaling machineries with multiple receptor components (Chiaruttini et al., 2008).

Tropo-myosine-related kinase (Trk) B is one of well characterized membrane components for BDNF receptors that are highly expressed in the nervous system (Klein et al., 1989). Its extracellular region consists of a signal peptide, two cysteine-rich domains, a cluster of three leucine-rich motifs, and two immunoglobulin-like domains, while its intracellular domain contains the tyrosine kinase domain (as illustrated in Fig. 5B). Thus far, three TrkB splicing variants have been identified in rat (Middlemas et al., 1991); a tyrosine kinase intact form (TK(+)) and two kinase truncated forms (TK(−): T1 and T2). T1 and T2 have unique short C-terminal amino acid sequences (T1, 11 residues; T2, 9 residues) instead of the tyrosine kinase domain of TK(+). TK(+) was identified in various species including mammals, chick, frog and zebrafish, and many studies have revealed the signal transduction pathways (Reichardt, 2006), expression profiles and functions. In mice, two kinds of TrkB gene knockout organisms have been generated (Klein et al., 1993; Luikart et al., 2003). One is *TrkB*$^{k}$(−/−), the TK(+) isoform-specific knockout mice, and the other is *TrkB*(−/−) to delete all TrkB isoforms in mice. Both mice were born alive but mostly died within 4 days because they were unable to take nourishment. *TrkB*$^{k}$(−/−) mice had cell loss in both the sensory and motor neurons and these phenotypes were severer than those in *Bdnf* gene knockout mice in which only the sensory neurons were affected. This indicated that TrkB uses other neurotrophins as its ligand in *in vivo* situations. In *TrkB*(−/−) mice, the cell loss phenotype of sensory

* Corresponding author. Fax: +81 42 346 1752.
*E-mail address:* kumanogo@ncnp.go.jp (H. Kumanogoh).

1044-7431/$ – see front matter © 2008 Elsevier Inc. All rights reserved.
doi:10.1016/j.mcn.2008.07.024

neurons was severer than that in *TrkB*$^{k}$(−/−) mice, particularly in those regions where survival of neurons is totally dependent on BDNF and neurotrophin-3, implicating functional relevance of multiple kinds of TrkB receptor isoforms other than the TK(+) isoform.

TK(−) variants had been assumed to simply play a dominant negative role on TK(+) (Eide et al., 1996; Haapasalo et al., 2001; Li et al., 1998). However, one of TK(−) isoform, TrkB-T1 receptor was identified in mouse, monkey, human and chick, and recently, others and we have shown that T1 isoform alone could activate a discrete signaling cascade in rat astrocytes; T1 has a direct signaling role in mediating inositol-1,4,5-triphosphate-dependent calcium release (Rose et al., 2003), and T1 isoform alone could activate a discrete signaling cascade by a cytoplasimic binding partner RhoGDI1 to reorganize cytoskeletons (Ohira et al., 2005). On the other hand, T2 isoform has been deposited to the public database only in rat. Two groups have reported T2 transcript and protein expressions: Armanini et al. reported that mRNAs encoding two truncated isoforms, TrkB-T1 and -T2, are differently distributed in the rodent nervous system, and each of these transcripts is co-expressed with TK(+) (Armanini et al., 1995). Silhol et al. demonstrated that T2 mRNA and its protein product gradually decreased from the postnatal day-7 becoming undetectable by 22-month-old in the rat hippocampi by the RNA protection assay and western blot analysis using specific antisera for rat T2 isoform, while physiological properties of T2 are still largely unknown. In any cases, *in vivo* roles of TK(−) remain uncertain (Silhol et al., 2005).

To further understand *in vivo* functions of TK(−) during mouse development, it would be important to identify those cell populations that express each TrkB isoform. In the present study, we extensively map mRNA expression patterns of BDNF and TrkB variants by a sensitive *in situ* hybridization (ISH) method. As the results, we found that TK(−) mRNA expression did occur in TK(+) negative cell populations both at the embryonic and postnatal stages. In addition, we realized differential expression profiles of T1 and T2 transcripts along the ventricular zone of the embryonic and postnatal brains. These results implicate novel and separable roles of TK(−) forms in regulating cell division and/or differentiation of the ventricular/ependymal cells. Furthermore, we found some bidirectionally transcribed regions located within an *Ntrk2* gene intron and identified novel TrkB splicing variants from one of the transcribed regions of *Ntrk2* by means of RT-PCR. Importantly, each expressed TrkB isoform in Neuro-2a cells appeared to be delivered to distinct subcellular domains and more or less affect cell shapes. These results highlight intricate modes of *Ntrk2* gene expression and multiple roles of TK(−) variants in neural development.

## Results

### *Confirmation of mouse Ntrk2 gene structure to design specific ISH probes for TrkB isoforms*

To investigate *in vivo* roles of TK(−), we first tried to precisely map the expression patterns of TrkB isoforms and their ligand, BDNF by means of a sensitive *in situ* hybridization (ISH) in the mouse nervous system. To obtain specific ISH probes for each TrkB receptor isoform, we referred to the UCSC genome browser (http://genome.ucsc.edu) and confirmed the structure of mouse *Ntrk2* gene locus that generates TrkB receptor isoforms. As was summarized in Fig. 1A, nine exons from the second to tenth only encode the extracellular (EC) region, the eleventh exon encodes both the EC and transmenbrane (TM) region (colored in red), the twelfth exon encodes the TM and a part of juxtamembrane region (JM) (colored in gray) and the last six exons (colored in pink) encode the tyrosine kinase (TK) domain containing cytoplasmic region of mouse TrkB-TK(+) isoform in the gene locus.

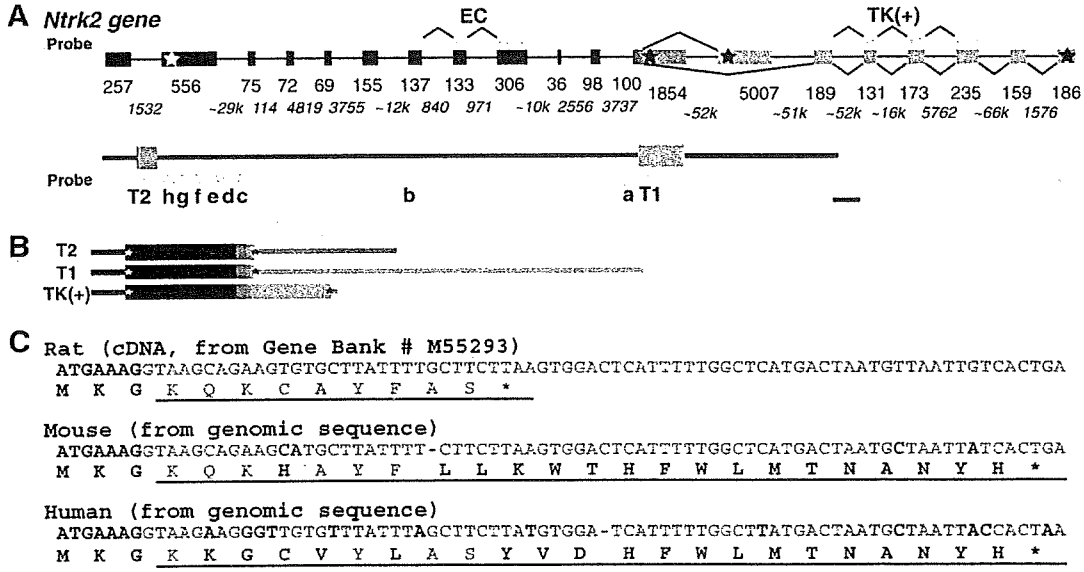


Fig. 1. Genomic organization of the *Ntrk2* (TrkB) locus and its alternative transcripts. (A) The upper illustration shows structure of the *Ntrk2* gene locus. Exons and introns are depicted as boxes and horizontal lines respectively. The alternative splicing patterns are represented by solid v-shapes connecting the exons. The numbers indicate their sizes by base pairs (those numbers in italics are for introns). Constitutive exons are specified as black, red and gray boxes, while alternative exons are shown as colored boxes: TK(+); pink, T1; green, T2; blue. The red and gray boxes show transmembrane and juxtamembrane region-coding domains, respectively. White and black stars show positions of the initiation and stop codons respectively. The lower drawing is a higher magnification between T2 and T1 exons. Bar represents 2 kb. *In situ* hybridization (ISH) probes in this study are indicated by orange boxes. Probes for the extracellular domain (EC) and TK domain (TK) cover coding regions straddling more than two exons. Probes a, b, c, d, e, f, g and h are positioned in the intron between the last constitutive exon and T1 exon. BDNF probe is against the part of the coding region (not shown). (B) Mature transcripts from the *Ntrk2* gene locus generated by alternative splicing. Translated regions are shown by colored boxes and untranslated segments are shown by colored lines. White and black stars show positions of the initiation and stop codons respectively. (C) Comparison of T2 amino acid sequences among species. Those amino acid (a.a.) sequences based on rat cDNA and mouse or human genomic DNA sequences are aligned. The constitutive exon and continuous T2 specific regions are shown in black and blue, respectively. Letters written in red indicate deletion or substitution nucleotides and distinct a.a. sequences compared with rat ones. T2 specific a.a. sequences are underlined. Note that putative T2 a.a. sequences are not well conserved among mammals.

Between the TM–JM specific exon and the first cytoplasmic specific exon of TrkB-TK(+), one alternative exon is annotated. This exon is shown by a green box in Fig. 1A, standing as a totally isolated alternative exon encoding T1 specific cytoplasmic tail. Based on the information, we selected those exonic regions encoding a part of TrkB extracellular immunoglobulin-like domains as the EC probe to detect all TrkB isoforms as was previously reported (Klein et al., 1989). T1 isoform-specific probe was prepared from its specific exon and TK probe was employed to avoid cross-react with other Trk family members as previously described (Armanini et al., 1995; McMahon et al., 1994).

In designing T2 isoform-specific probe, we initially referred to the cDNA sequence that was only reported in rat (Middlemas et al., 1991): we found that the rat T2 specific exon is located at the 3′-flanking region of the last TrkB constitutive exon (=TM–JM specific exon) without any intronic gaps. Synthesis of mature mRNAs for rat TrkB splicing variants has therefore been assumed as follows; immature RNAs are first transcribed from the rat *Ntrk2* gene locus, then constitutive exons (as shown with black boxes in Fig. 1A) and alternative exons, namely T2 (a blue box in Fig. 1A), T1 (a green box in Fig. 1A), or TK (pink boxes in Fig. 1A), are selected by splicing, and mature T2, T1 or TK(+) mRNAs are finally synthesized, respectively (the schematic drawings of spliced mature mRNAs were shown in Fig. 1B). We next predicted mouse and human putative T2 amino acid sequences from their genomic sequences based on the rat T2 exonic position, and these deduced amino acid sequences were compared with the rat T2 protein tail structure. Unexpectedly, these isoform-specific amino acid sequences and lengths were totally different as shown in Fig. 1C; rat; 9 amino acids, mouse and human; 23 amino acids, while T1 tail structure was well conserved among mouse, rat, human, monkey and chick (data not shown). This indicates a possibility that T2 transcript is merely a part of premature mRNAs for other TrkB isoforms and is not to be translated to the protein at all. ISH probe for mouse T2 segment was hence prepared from the mouse genomic sequence corresponding to rat T2 genomic position. We additionally developed two intronic probes a and b to compare the expression profiles with those obtained by T2 probe. One of intronic probes, probe a, covers the 5′-flanking region of T1 exon and the other, probe b, is situated in the middle of two exons (Fig. 1A). To gain identical level of signals in case these intronic regions and T2 segment have equal level of expressions, we conferred same length and UTP ratio to these probe sequences. By using these probe sets, we could determine if T2 is a part of immature mRNA for other TrkB isoforms or not, as the T2 specific region is considered to be a portion of the intron between the last 3′-constitutive exon and T1 exon. For instance, T2 segment is considered as a part of the intron when these two intronic probes yield the same signal levels as T2 probe. T2 segment is regarded as an exon for a TrkB isoform when T2 expression profile is totally different from expression signals detected with these two intronic probes.

### *Distinct expression profiles of TrkB isoforms and BDNF during mouse development*

We compared the expression patterns of BDNF, TrkB isoforms; TK(+), T1, T2, two intronic regions (a and b) and all TrkB isoforms detected by the EC probe at the three mouse developmental stages, embryonic 12.5-day (E12.5), postnatal day-7 (P7) and 8-week-old (8W) by means of ISH on serial sections (Figs. 2 and 3). Their differential expression domains as well as their intracellular distributions were summarized below.

#### *TK(+) specific probe*

In a frontal section of the E12.5 embryo (Fig. 2A), TK(+) specific signals were not detected in the vicinity of the ventricular zone (VZ) of midbrain and spinal cord, which is totally different from T1 or T2 expression profiles (as described below). TK(+) specific staining instead delineated the ventral mantle zone and subsets of neurons in the dorsal root ganglion (DRG). At the postnatal stages, TK(+) signals were highly detectable in the cerebral cortex (Fig. 3), hippocampus, thalamus and cerebellum (data not shown) as described previously (Dugich-Djordjevic et al., 1993). The signal level at P7 was higher than that at 8W, which is consistent with earlier descriptions (Fryer et al., 1996). At the cellular level, ISH staining signals were always found within the peri-nuclear/cytoplasmic compartment at all stages examined, indicating that these signals are all derived from mature mRNAs.

#### *T1 specific probe*

T1 specific signal was distributed in the ventral ventricular side of the midbrain at E12.5 (Fig. 2A). In the rest part of the central nervous system at this developmental stage, the whole VZ was intensely stained by T1 probe. In addition, we found conspicuous stainings at the roof plate (RP) of the spinal cord and emigrating neural crest cells from the RP (Fig. 2B). Nerve associated cells and DRG satellite cells were also demarcated by T1 expression at E12.5. At the postnatal stages, T1 mRNA was strongly expressed in the ependymal cells of all the brain ventricles (Fig. 3 and data not shown) (Dugich-Djordjevic et al., 1993). Noticeable was the fact that intracellular distribution of T1 signal in the ependymal cell population was cytoplasmic and appeared to be actively concentrated at the ventricular side. The T1 specific signals also distributed diffusely in the cerebral cortex, Purkinje cell layer and granule cell layer of cerebellum at adult stage (data not shown), which may reflect T1 expressions in astrocytes (Ohira et al., 2007). T1 expression level was developmentally increased in the cortex and cerebellum as described previously (Fryer et al., 1996).

#### *T2 specific and intron probes*

T2 specific probe detected strong signals in the VZ of the midbrain with their staining being localized around the peri-nuclei and T2 showed distinct expression patterns at E12.5 (Fig. 2A, shown with black stars and triangles): Comparing with T1 distribution, T2 was uniquely distributed in the medial mantle zone of the midbrain (Fig. 2A). On the other hand, the intron probes stained similar regions detected with T2 probe but the staining level was weaker than T2 one at E12.5 (Fig. 2A, depicted with black, gray and white triangles). At P7, signal distribution patterns and intensities obtained from the T2 probe became equal to those from probes a and b. Intracellular distributions of these signals were found in the nuclei or at the nuclear membranes around the VZ (Fig. 3A) and cerebellum (data not shown), indicating that these are not all derived from mature mRNAs. At 8W no labeling was detected around the VZ (Fig. 3B) with T2 probe, probes a and b, while they yielded similar signal intensities and intracellular distributions in the adult cerebellum (data not shown). Sense probes for T2, regions a and b did not give any specific signals at all the stages and tissues tested (data not shown). These results suggest that the T2 territory codes one of TrkB isoforms with relevant functions in the expressed areas at E12.5, while the territory only remains to be a part of premature mRNA/intron for other TrkB isoforms at the postnatal stages.

#### *BDNF specific probe*

BDNF mRNA was strongly expressed in the trunk epidermis (Fig. 2A) and cranial spiral ganglia (data not shown) at E12.5. At P7, BDNF signal was detected in the CA3 of the hippocampus, mammillary nuclei and other regions previously reported (data not shown). We also confirmed the intense ISH signals in the CA3 and dentate gyrus of the hippocampus and piriform cortex at 8W (Conner et al., 1997). Moderate level of BDNF expression was further observed in the CA1 of the hippocampus, cortex and granule cell layer of the cerebellum at this stage (data not shown) as was described previously. At the cellular level, almost all signals were found distributed to cytoplasmic compartments (data not shown).

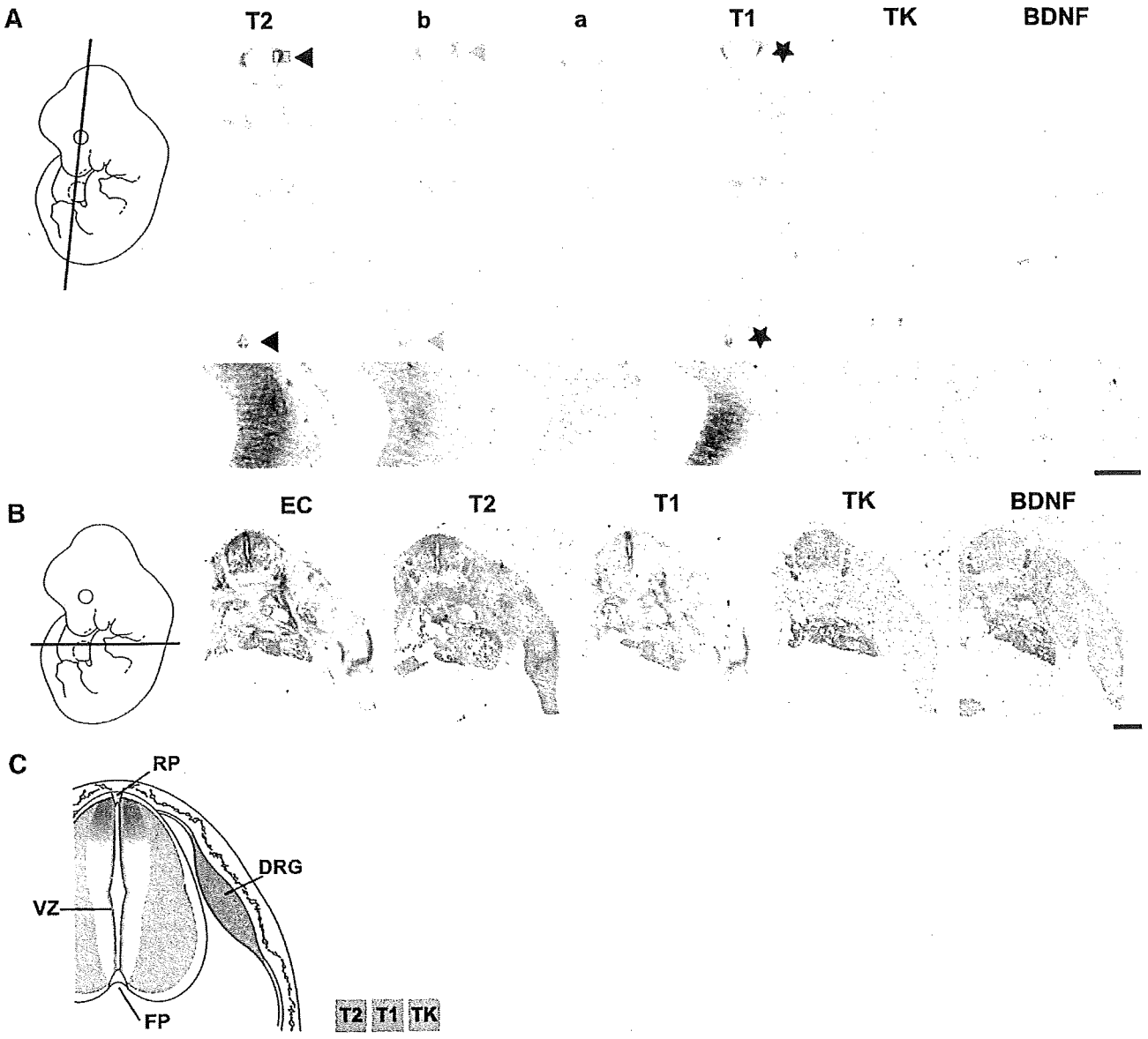


**Fig. 2.** Dynamic regulation of *Ntrk2* gene expression in the mouse nervous systems at embryonic day (E) 12.5. (A) The upper panels; ISH staining results from mouse E12.5 embryo frontal serial sections are arranged. The section plane is indicated by a line in a schematic drawing of the E12.5 embryo and probes applied are specified above. The lower panels show a high magnification of the boxed area in the upper panels. Note that probes a and b yield only weak stainings compared to specific signals from T2 probe as depicted by triangles (black ones, intense expression; gray ones, intermediate level of expression; white ones, weak expression). T1 probe also stained different regions compared with T2 positive domains. (as shown by stars). Bar indicates 1 mm and 50 μm for the upper and lower panels, respectively. (B) Coronal sections of an E12.5 embryo containing the neural tube are serially collected and processed by ISH, whose results are arranged in the panels. The section plane is indicated by a line in a schematic drawing of the E12.5 embryo and probes used are specified above. Note that T2, T1 and TK signals have different distributions around the ventricular zone. Bar, 500 μm. (C) Summary of T2, T1 and TK(+) expressions in the E12.5 nervous system. Expression domains for T2, T1 and TK(+) are painted with blue, green and pink respectively. T1 signals are distributed in the ventricular cells of the neural tube, roof plate (RP) and migrating neural crest cells. T2 signals delineate the dorsal side of the ventricular zone (VZ) and cells in the dorsal root ganglia (DRG). TK signals demarcate the lateral side of the VZ and only subsets of neurons in the DRG. FP, floor plate.

*Comparison of TrkB isoforms and BDNF expressions in the spinal cord at E12.5*

As described above, TrkB isoforms appear to differentially demarcate cell populations around the spinal cord at E12.5. To compare TK, T1 and T2 expression patterns more precisely, we performed ISH on serial coronal sections of the spinal cord at E12.5 (Fig. 2B). Consequently, we found that T1 signals were dominantly distributed to the ventricular cells of the neural tube, roof plate and migrating neural crest cells. T2 signals delineated the dorsal side of the VZ and almost all cells in the DRG. TK signals demarcated the lateral side of the VZ and only subsets of neurons in the DRG. These expression domains of TrkB isoforms around the neural tube were illustrated in Fig. 2, highlighting differential expression and roles.

Collectively, we suggest that T2 territory is processed to mRNA encoding a TrkB isoform only at E12.5 but T2 becomes a part of the intron at the postnatal stages. The hypothetical mechanisms of T1 and T2 transcript synthesis are shown in Fig. 3C (see details in Discussions), and that *Ntrk2* gene transcriptional mechanism may be dynamically changed before and after birth.

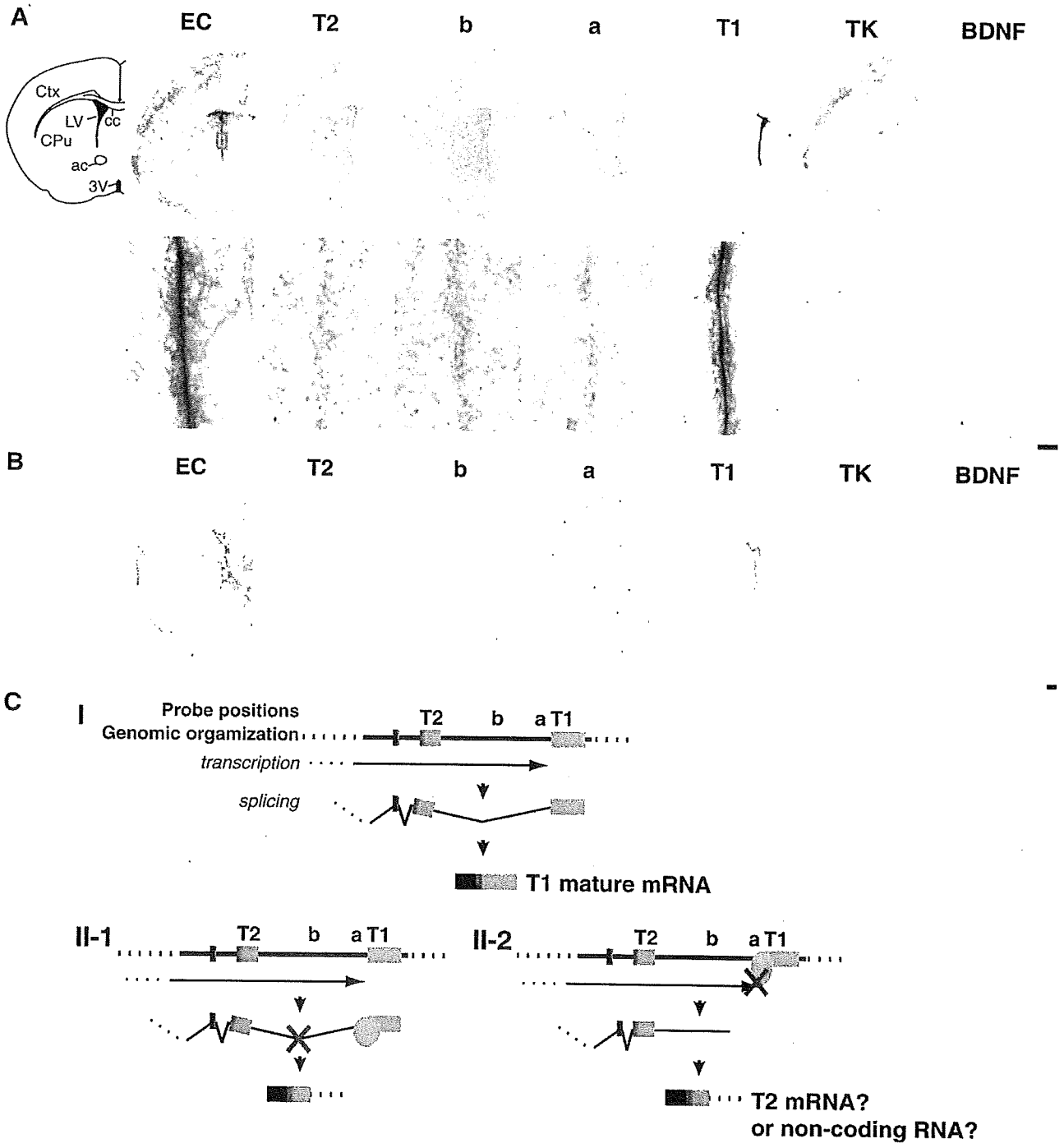


**Fig. 3.** Dynamic regulation of *Ntrk2* gene expression in the ventricular zone at postnatal stages. (A) The upper panels represent staining results of postnatal day-7 (P7) mouse frontal brain sections with a low magnification. The section appearance is indicated by a schematic drawing. ac, anterior commissure; cc, corpus callosum; CPu, caudate putamen; Ctx, cortex; LV, lateral ventricle; 3V, 3rd ventricle. The lower panels show a high magnification of the boxed area in the upper panels. Staining signals by T2, probe b and a distribute at the nuclear membrane with the identical pattern and intensity. Bar represents 500 μm and 50 μm for the upper and lower panels, respectively. (B) Panels represent results of 8-week-old mouse brain ISH with indicated probes. Note that signals are not detected by probes T2, b and a. Bar, 500 μm. (C) Hypothetical mechanisms of alternative T1 and T2 mRNA synthesis. I. The intron including probe regions T2, b and a is spliced out, and mature T1 mRNA is synthesized. This mechanism is dominantly activated in T1 expressing regions. T2 mRNA or non-coding RNAs are synthesized because a splicing blocker binds to the premature T1 mRNA (II-1) or a transcriptional blocker binds to the 5′-flanking region of T1 exon (II-2). At E12.5 the mechanism II is in action for T2 positive regions by ISH and the mechanism I is applicable to T1 expressing regions, while at postnatal stages only mechanism I is activated.

*The 3′-flanking genomic segment of TrkB-TM/JM-T2 exon was dynamically transcribed in the mouse nervous system*

To further clarify the transcriptional mechanisms of mouse *Ntrk2* gene locus, we focused on the 3′-flanking region of TrkB-TM/JM-T2 exon and prepared specific probes for six genomic segments, namely regions c, d, e, f, g and h. We then rigorously examined the expression profiles by means of ISH at E12.5 and P7 stages (Fig. 4). Relative positions for these segments were drawn in Figs. 1 and 6 with their sense and antisense orientations being defined along the *Ntrk2* gene/

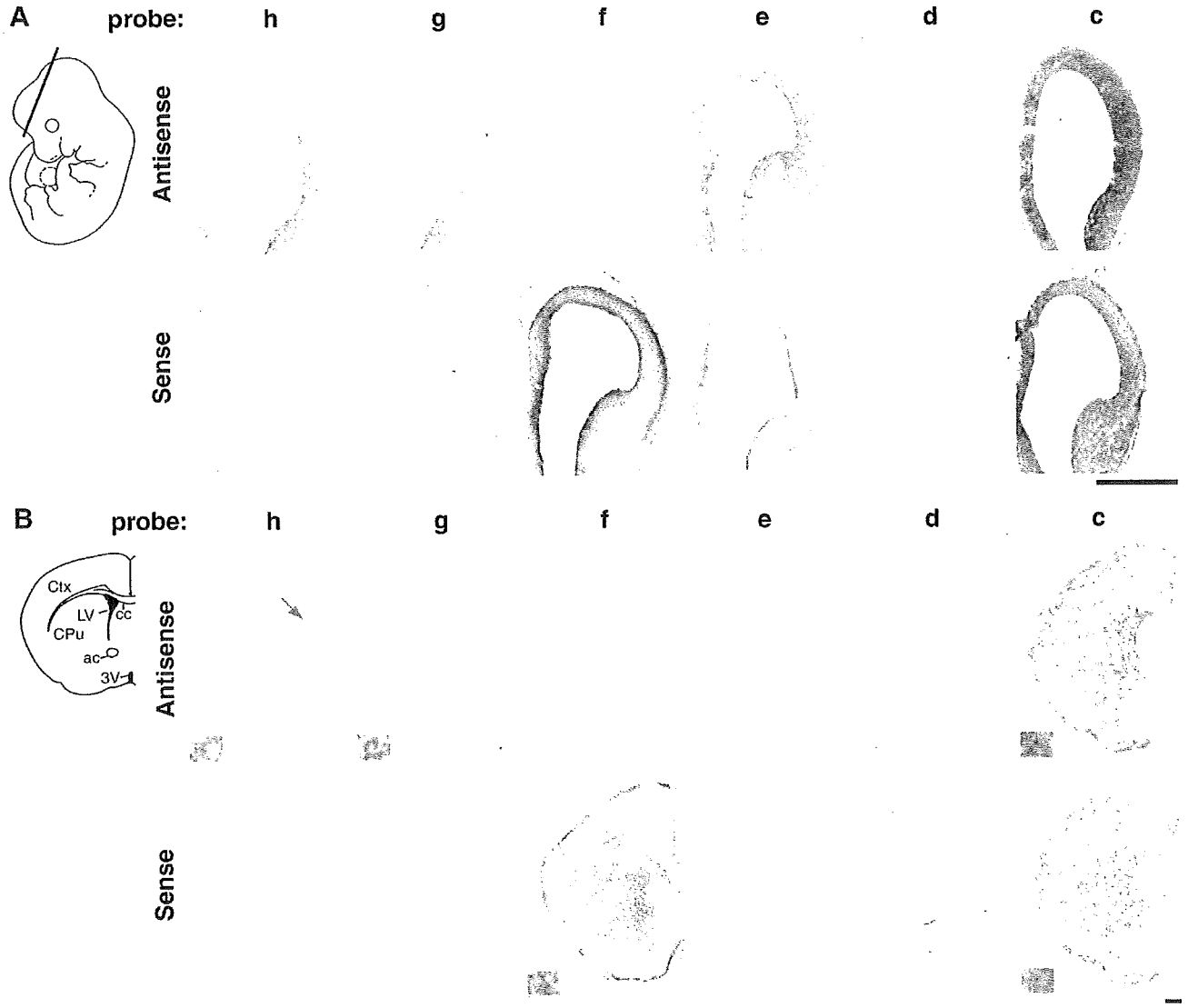


Fig. 4. Multiple territories in the 3′-flanking region of T2 specific exon in the *Ntrk2* gene locus is differentially expressed in the nervous systems. (A) The panels represent ISH results of mouse embryo at E12.5. Probe regions are summarized in Figs. 1 and 6. The upper panels represent staining results with h, g, f, e, d and c antisense probes (AS). The lower panels show staining patterns with their sense probes (S). The section plane is indicated by a line in a schematic drawing of the E12.5 embryo. Bar, 500 μm. (B) The panels represent ISH results of coronal brain sections at P7. The upper panels represent staining results with h, g, f, e, d and c antisense probes (AS). The lower panels show staining patterns with these sense counterparts (S). The section appearance is indicated by a schematic drawing. The inset of each panel shows a high magnification around the ventricular zone pointed by the orange arrow. Note that AS-probes for h, g and d and S-probe for f yield signals however opposite probes have no staining. AS- and S-probe c generate intense signals. Bar signifies 400 μm for the brain sections and 15 μm for the insets. ac, anterior commissure; cc, corpus callosum; CPu, caudate putamen; Ctx, cortex; LV, lateral ventricle; 3V, 3rd ventricle.

TrkB protein coding direction. As was summarized below, their transcriptional directions and expression domains were extremely intricate during brain development, although these six segments are confined within a 7 kb genomic territory.

*Probes for region g and h*

Regions g and h appeared to yield similar expression profiles at E12.5 and P7. Their antisense (AS)-probes were mainly detected in the ventral side of midbrain VZ (Fig. 4A), prospective cerebral cortex and cochlear nucleus (data not shown) at E12.5. Their signals were intense and showed perinuclear foci at the cell level. As contrasted with the AS-probes, their sense (S)-probes did not detect any expression at E12.5. In P7 brain sections, the AS-probe signals were distributed around the VZ of lateral ventricle (Fig. 4B insets), cerebral cortex (Fig. 4B) and cerebellum (not shown) yet the S-probes did not yield any staining signals. Considering the relative positions in the genome, these two regions may generate a continuous transcript.

*Probes for region f*

From this genomic segment, the S-probe but not the AS-probe detected RNA expression at E12.5 and P7. The S-probe signals were intense at both the ventricular and marginal zones of the telencephalic

Fig. 5. Nucleotide sequences and deduced amino acid sequences of two novel splicing variants. (A) Two novel splicing variants (T3 alpha and beta) are identified by RT-PCR. The cDNA sequences and deduced amino acid (a.a.) sequences are shown. The predicted transmembrane a.a. sequences are underlined. Novel TrkB-specific a.a. sequences are enclosed by purple boxes. (B) The putative protein structure of new TrkB splicing variants are aligned with those of TK, T1 and T2.

A

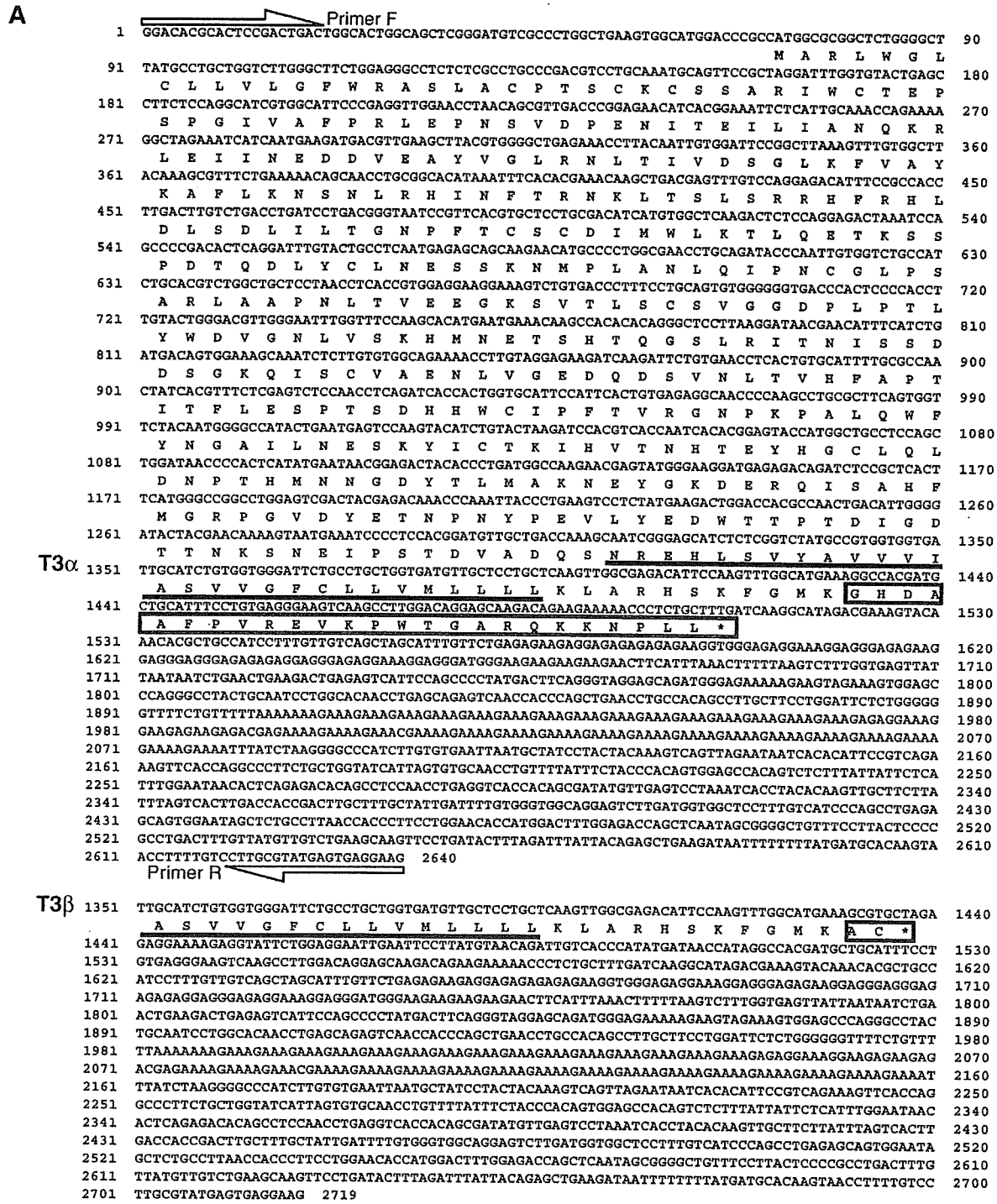
Primer F
T3α
Primer R
T3β

B

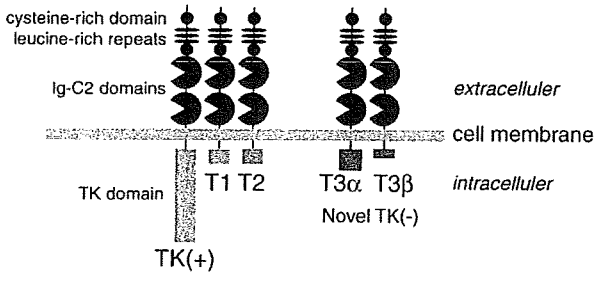
cysteine-rich domain
leucine-rich repeats
Ig-C2 domains
extracelluler
cell membrane
TK domain
T1 T2
T3α T3β
intracelluler
Novel TK(-)
TK(+)

vesicle (Fig. 4A) at the embryonic stage. At P7, the S-probe signals were strongly detected only at the marginal zone of cerebral cortex (Fig. 4B). The pia mater was also marked by the S-probe. Their intracellular signals were all in the nuclei, indicating these signal are not derived from mature types of mRNA.

*Probes for region e*

Both chains of this genomic segment were expressed at E12.5, but their expression patterns were diverse. The AS-probe signals were intensely detected at the ventral ventricular side, which is very similar to the staining patterns obtained by the AS-probes g and h. The S-probe yielded the expression profiles resembled with those detected by the aforementioned S-probe f (Fig. 4A). At P7 no signal was observed in the brain by both probes (Fig. 4B), implicating developmental stage specific activation of this genomic segment.

*Probes for region d*

The AS-probe detected faint signals in the ventral ventricular side of the telencephalic VZ at E12.5 and the distribution patterns were just like those obtained by the AS-probes g, h and e, while the S-probe did not detected any evident signals at this stage (Fig. 4A). At P7, the AS-probe yielded weak signals around the VZ, while the S-probe did not detect any staining signals (Fig. 4B).

*Probes for region c*

Both the S- and AS-probe detected extremely intense signals, marking a broad variety of cells in the nervous system. In the E12.5 telencephalic vesicles, the AS-probe strongly stained almost all cell populations including the VZ, while the S-probe gave a negative area at around the ventral mantle zone (Fig. 4A). At the cellular level, almost all signals were distributed in the cytoplasm. In some regions, the S-probe signals were detected in the nuclei at the embryonic stage, while the AS-probe signals were found in the cytoplasm. The bidirectional transcription was also observed widely at P7 and all of their intracellular distributions were in nuclei. One clear difference among their expression patterns was found in the ependymal cell layers of the lateral ventricle where only the AS-probe yielded strong staining signals (Fig. 4B).

In summary, although T2 and regions c, d, e, f g, and h were positioned within a 10 kb genomic region, their expression patterns and timing, intracellular distributions and transcriptional direction were extremely variable. These results indicate that the expression of these regions in *Ntrk2* gene locus is strictly regulated and each transcript could harbor important roles.

*Identification of novel alternative splicing variants encoding truncated isoforms for TrkB receptor*

Since intense ISH signals were detected with probes from region c both at E12.5 and P7, we assumed that the sense transcript from region c is a part of unknown alternative splicing variants of TrkB. We first examined whether cDNA that contains both sequences from the TrkB constitutive exons and region e, d, or c is present. We attempted to amplify such transcripts from the cerebral cortex, cerebellum or liver cDNAs at P7 by means of RT-PCR. For the primer, we designed three forward primers positioned in the TrkB constitutive exons (F1, F2 and F3 in Fig. 6) and reverse primers match to region e, d, and c (R1, R2, R3 and R4 in Fig. 6) or the 5′ flanking region of the 3′-proximal polyadenylation signal sequence from region c (Primer R in Fig. 6). As expected, prominent products were amplified from the cerebral cortex or cerebellum cDNA when we used the reverse primers within region c (R3 or R4) or Primer R. Lengths of these PCR products changed according to positions of the forward primer and were clearly shorter than those of genomic fragment, indicating some introns exist in the genomic region between the TM–JM exon and Primer R (data not shown). We next tried to identify splicing sites in the genomic region. To this end, one PCR product highly amplified by one of the forward primers, F1 and Primer R was cloned into pGEM-T Easy vector and fourteen clones obtained were sequenced with the forward primer F3 located in the TM–JM exon. Consequently, we found that these clones could be divided into two groups by means of their splicing pattern (Figs. 5 and 6): Eleven of these had T3 alpha-type splicing, and the remainder had T3 beta-type splicing. We then re-amplified their full-length cDNAs by the forward primer positioned at the 5′-side of the initiation codon (Primer F) and Primer R and cloned them into the vector. Sequences of their cDNA and deduced amino acids, summarized in Fig. 5, suggested that the cDNA could encode novel types of TrkB-TK(−) receptors. These sequence data have been submitted to the DDBJ databases under accession No. AB377224 for T3 alpha and AB377225 for T3 beta. Briefly, TrkB-T3 alpha variant had 24 specific amino acids in cytoplasmic tail, while TrkB-T3 beta isoform harbored specific tail with two amino acids. Incidentally, T3 alpha specific tail was not conserved among species just as the putative T2 specific cytoplasmic tail, whereas the short T3 beta tail was well conserved

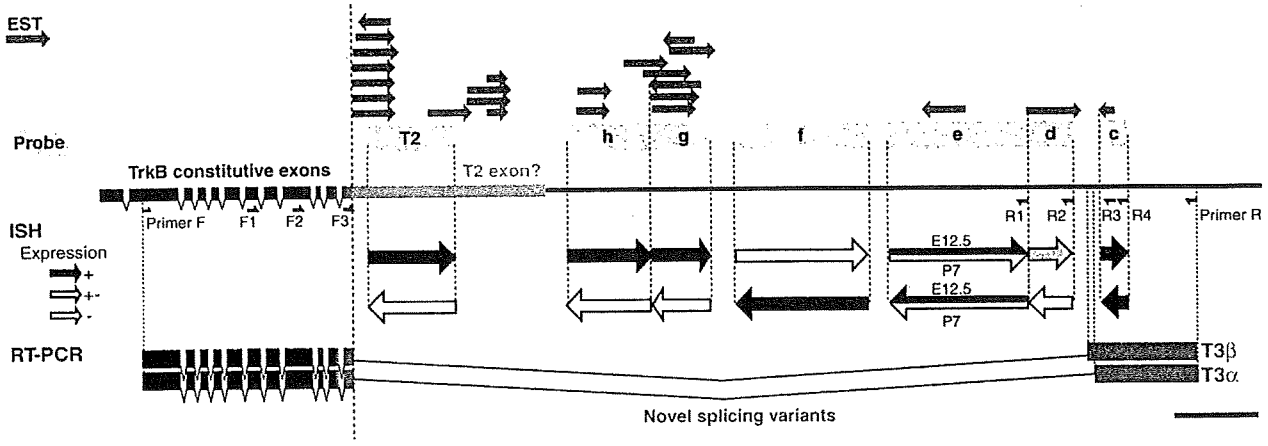


**Fig. 6.** Summary of transcripts from the 3′-flanking region of T2. In the upper part of the figure, mouse ESTs in the UCSC database are shown by red arrows and probes for ISH are specified by orange boxes. The constitutive exons are indicated by black boxes and the 3′-flanking genomic region of the last constitutive exon is depicted by a bold line with the putative T2 exon colored by light blue, and primers used in this study are depicted. The middle part outlines ISH results by bold arrows and their colors indicate signal intensity; intense (black), weak (gray), none (white). New splicing variants confirmed by our RT-PCR are summarized in the lower part of the figure. Note that those territories annotated by ESTs coincide with the transcribed genomic regions. Bar, 1 kb.

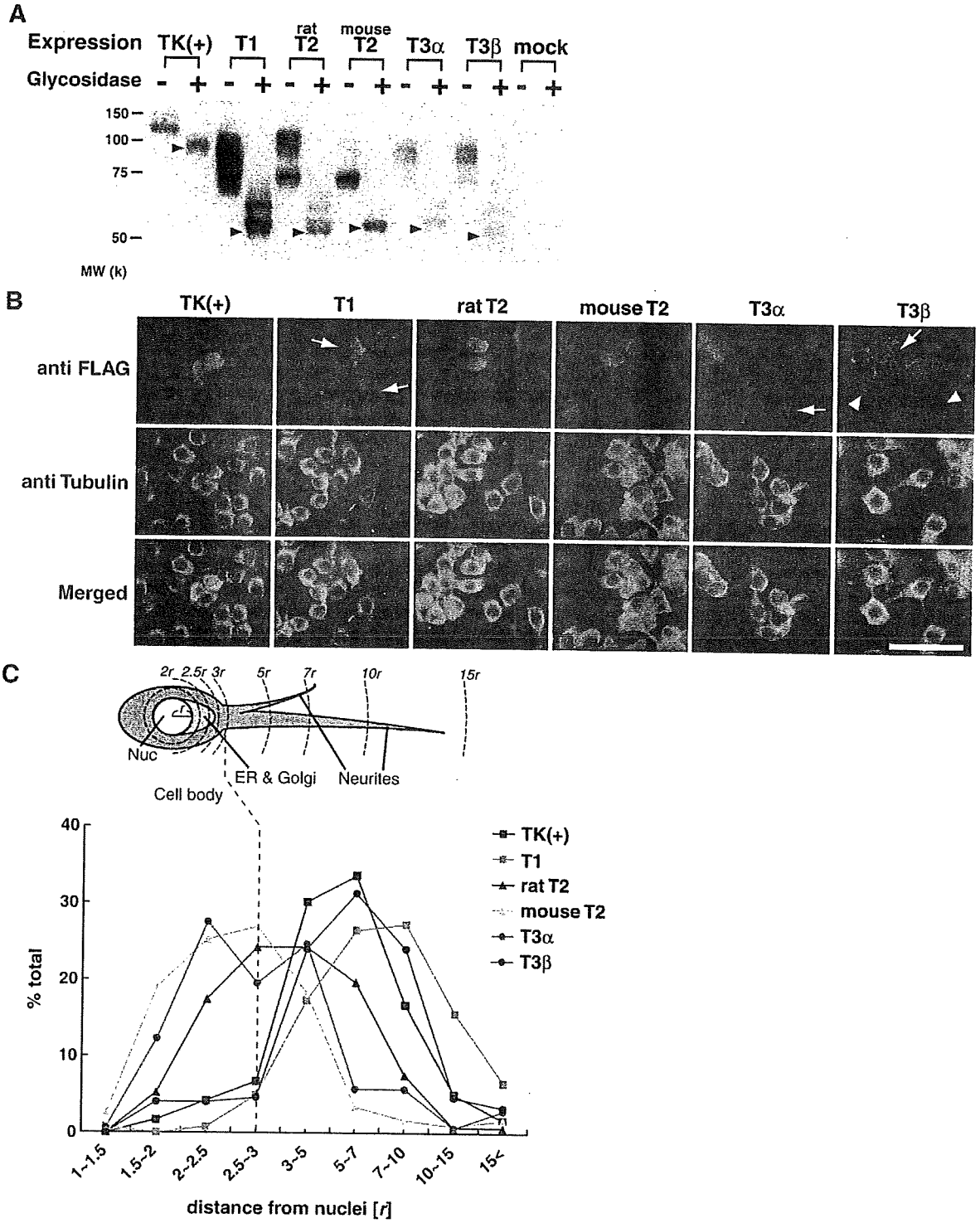


Fig. 7. Different effects from expressed TrkB variants in Neuro-2a neuroblastoma cells. (A) Western blot analysis of FLAG-tagged TrkB variants in Neuro-2a cells. Cell lysates are incubated with (+) or without (−) *N*-Glycosidase F and equal volume of those samples are analyzed by immunoblot with anti-FLAG polyclonal antibody. The apparent molecular weights of deglycosidated TrkB variants are almost identical with the predictive ones (arrowheads). Mock, transfection with expression vector alone. (B) Intracellular distribution of FLAG-tagged TrkB variants in Neuro-2a cells. Cells transfected with FLAG-tagged TrkB variant constructs are immunostained with anti-FLAG antibody (red) and anti-Tubulin antibody (green). Arrows and arrowheads indicate typical distribution patterns and/or effects of each isoform (see Results section). Bar, 50 μm. (C) Each expressed TrkB variant exhibits characteristic response in Neuro2a cells. The upper scheme shows the morphological model of a cell where the radius of the nuclear structure is defined as *r*. We measured the maximum distance from the center of nucleus to the cellular edge among hundreds of parental cells to find the cell body is always included within the circular area with the radius being 3*r* (showed by the broken line spanning the panels) and all the neurite extensions occurring outside of the 3*r* area. Nuc; nucleus, ER & Golgi; endoplasmic reticulum and Golgi apparatus (orange color). The lower graph shows how TrkB variants are expressed by analyzing the distribution pattern along the cellular/neurite extensions. Note that each variant yields a unique graph pattern. The vertical axis, percentages of cell number within the defined circular area; the horizontal axis, distances from the center of cell nuclei measured by *r*.

among mouse, human and dog genomic sequences from the UCSC database (data not shown).

*Strict expression and response of TrkB variants in Neuro-2a neuroblastoma*

To examine whether the various TrkB transcripts including rat/mouse T2 and novel mouse T3 alpha/beta isoforms encode functional proteins, we sought to transfect their cDNAs into the cultured cells to harbor the FLAG tag at the N-terminus of mature proteins if expressed. To avoid the influence of intact TrkB protein, we adopted Neuro-2a cells which do not express endogenous TrkB (Haapasalo et al., 1999).

At first, we analyzed the expressed TrkB proteins with western blotting. One day after transfection with those tagged constructs, cell lysates were prepared and treated with *N*-Glycosidase F to identify the precise molecular weights of glycosilated TrkB proteins. Consequently, all TrkB variants transfected were found to be detectable with anti-FLAG antibody (Fig. 7A) or anti-TrkB antibody (data not shown) and their apparent molecular weights were identical with their calculated ones (92.1, 53.2, 53.0, 54.5, 54.7 and 52.1 k for TK(+), T1, rat T2, mouse T2, T3 alpha and beta; Arrowheads of Glycosidase+ lanes in Fig. 7A). Thus, TrkB variants were confirmed to be accurately expressed in Neuro-2a cells.

Next, we analyzed the intracellular distribution of TrkB isoforms by anti-FLAG antibody, where anti-Tubulin antibody was simultaneously utilized to visualize the morphology of transfectants (Fig. 7B). As the results, we found that each isoform was differently distributed in the transfectant. To further evaluate those differences in details, we measured the distance from the center of nuclear structure to the most distal staining signal of anti-FLAG antibody in each cell. More than 100 transfectants per one isoform were analyzed and categorized as shown in the upper drawing of Fig. 7C (see details in Experimental methods). As a consequence, we noticed that TK(+) distributed along the neurites (the distance over 3*r*: ~90%). Regarding the T1-isoform, almost all proteins were transported to the distal processes (the distance over 3*r*: ~90%, Fig. 7C) and T1-expressing cells more or less changed their morphology to increase the number of filopodia and processes, sometimes flattening the whole shape (Fig. 7B, arrow), which is consistent with earlier studies (Haapasalo et al., 1999; Hartmann et al., 2004). In contrast, rat and mouse T2 isoforms were mainly distributed to the cell body and proximal neurites without morphological changes (the distance under 5*r*: ~70% for rat T2, ~90% for mouse T2). One of the novel splicing variants, T3 alpha was accumulated at the peri-nuclear structures including the Golgi apparatus in ~40% of the cells (Figs. 7A; arrow, and C; the distance under 2.5*r*), while another ~40% of cells harbored this expressed isoform along the neurites longer than 3*r*, resulting in an M-shaped graph by our analysis (Fig. 7C). T3 beta was transported into the neurites (the distance over 3*r*: ~90%) and the protein distribution pattern analyzed in Fig. 7C was similar to the case of TK(+) at a glance. However, T3 beta-expressing cells displayed flat-shape and increased processes, which rather resembles the case of T1 (Fig. 7B, arrow). T3 beta positive neurites occasionally surrounded the neighboring cells, which is very characteristic to this isoform (Fig. 7B, arrowhead). Taken together, each TrkB isoform was uniquely distributed in a cell and some of variants, T1 and T3 beta, altered the host cell shapes, suggesting that TrkB splicing variants with specific expression profiles may have distinct functions in the developing nervous system.

## Discussions

In the present study, we have shown that TrkB isoforms and BDNF are dynamically and differentially expressed in the developing mouse nervous system. Especially, we have demonstrated the possibility that the TrkB-T2 segment is expressed as mRNA at E12.5 yet becomes a part of intron after birth. In addition, we found that mouse *Ntrk2* gene locus is actively regulated to generate multiple transcripts, two of which could encode novel TrkB-TK(−) splicing variants. These results implicate complex ways of splicing and separable functions of mouse *Ntrk2* gene in the nervous system.

*Balanced ways of splicing to generate TrkB-TK(+), T1 and T2 isoforms from the mouse Ntrk2 gene locus*

We have demonstrated that expression domains of TrkB-TK(+), T1 and T2 are distinct with minimum overlaps in the nervous system and that ISH signals obtained from antisense probes for T2 specific segment are totally dissimilar to those for the continuous intronic segments at the embryonic stage. On the other hand, at the postnatal stages, probes from T2 specific segment and continuous intronic segments all yield similar levels and patterns of ISH staining with maximum overlaps in the nervous system. At the cellular level, distribution and intensity of T2 specific signals are almost equal to those obtained from the intronic probes and all their staining signals were not found in the cytoplasm. These results suggest that T2 specific segment is transcribed as mRNA at the embryonic stages and becomes a part of premature mRNA for other TrkB isoforms at the postnatal stages. How can these spatiotemporally regulated expressions from the *Ntrk2* gene locus be achieved?

We hypothesize balanced regulatory mechanisms in synthesizing T1/TK(+) and T2 transcripts from *Ntrk2* gene locus as is summarized in Fig. 3C: Within those cells specifically express TrkB-T1 or -TK(+), T1 and/or TK(+) mRNAs are dominantly synthesized by splicing out the intron that includes the T2 coding region as is shown in Fig. 3CI. Transcripts including the T2 coding region, regions b and a therefore stand as premature T1 and/or TK(+) mRNAs to be localized in cell nuclei or bind to the nuclear membrane. Within those cells strongly express TrkB-T2 mRNA, transcripts including the T2 coding region become dominant, while T1 and/or TrkB-TK(+) mRNA synthesis is inhibited at the level of splicing (Fig. 3CII-1) or transcription (Fig. 3CII-2). It is still uncertain that transcripts including the T2 coding region are effectively translated into TrkB-T2 protein. Yet if they generate stable protein products, these must exist as one of TrkB isoforms with separable functions other than simple dominant negative molecules to TrkB-T1 and/or -TK(+), since the expression is balanced to produce a defined TrkB isoform in a cell. Whatever the case might be, *Ntrk2* gene transcription mechanism would dynamically change before and after birth. Can this mechanism stand with earlier results?

Armanini et al. have previously shown the expression patterns of TrkB isoforms by ISH using $^{35}$S-labeled riboprobes in the E10.5, E13.5 and E15.5 spinal ventral horns and adult hippocampi. Our results are comparable to theirs at the embryonic stages, while we can additionally map the expression profiles with a higher resolution by our sensitive ISH system as illustrated in Fig. 2B, finding out that mouse TrkB-T1 is expressed in the neural crest generating zones (RP) and emigrating subpopulations from the RP. In the adult mouse hippocampi, Armanini et al. have noticed that both TK(+) and T2 specific transcripts are expressed in neuronal cells, yet in our results, T2 signals are not detected in these cell populations at all, while TK(+) and T1 distributions are comparable to theirs (data not shown). Silhol et al. have independently demonstrated that T2 mRNA and its protein product gradually decreased from the postnatal day-7 becoming undetectable by 22-month-old in the rat hippocampus. In light of the non-conserved structure of T2 among species as well as our data demonstrating that mouse T2 may functions as a protein only at embryonic stages, it should rigorously be examined if mouse and/or rat T2 protein is stably expressed in the mature nervous system by using specific antibodies.